LAMINATION AND MIXING IN CANONICAL AND TURBULENT FLOWS

L. Rossi , D. Doorly, A. Durant, D. Kustrin, S. Lardeau
Imperial College London
London United Kingdom
l.rossi@imperial.ac.uk or rossi_lionel@yahoo.fr

F. Schwander
Ecole Centrale Marseille
Marseille France

ABSTRACT

Lamination and mixing properties are characterised for a canonical flow (cat's eyes flip) at low Reynolds number ($Re{\sim}13$) and a turbulent flow. The cat's eyes flow is experimentally driven by electromagnetic forces while the turbulent flow is generated using 2D DNS. It is shown that lamination and stretching grow exponentially for both flows with an exponent higher for the stretching than for the lamination. Noticeably, the difference between the stretching and lamination exponents is higher for the turbulent flow than for the low Reynolds number flow with ratios respectively about 1.32 and 1.12. Moreover, lamination enhances mixing locally by reducing the distance over which diffusion needs to act to finalise mixing. The difference in the mixing properties of the flows is related to the distribution of lamination. The turbulent flow saturates locally, i.e. it reaches locally high lamination values where diffusion can act swiftly over short distances to finalise mixing while most of the flow is still with low values of lamination. This leads to an algebraic growth of the mixing coefficient. The cat's eyes flip flow globally increases lamination with a better space filling than the turbulent flow. This delays the saturation of mixing and leads to an initial exponential growth of the mixing coefficient.

INTRODUCTION

The aim of this paper is to explore lamination and mixing in canonical and turbulent flows. By canonical flows we mean simplified flows with selected generic properties. This is in the spirit of recent works using a multi-scale arrangement of counter jets with turbulent-like properties (Rossi et al., 2006a, Rossi et al., 2006b) and a single pair of jets to generate different flow geometries (Rossi et al., 2009). For the purpose of this paper, the chosen canonical flow is a flipping cat's eyes. Similar and complementary sequences are used in recent works on low Reynolds number mixers, e.g. (Rossi et al., 2011a, Rossi et al., 2011b).

An important property of flows is their ability to laminate material elements. It is well known that combinations of stretching and folding can produce exponential growth of interfaces as illustrated by the baker process, (Reynolds, 1893, Wiggins and Ottino, 2004). Moreover, if a laminated structure (e.g. dye concentration pattern) is subsequently exposed to a high strain domain, the distance between the striations can be reduced, leading to an increase in concentration gradients and diffusion between the different layers, e.g. (Rossi, 2010). Whilst the design and control of such mechanisms may be crucial to enhance mixing in low Reynolds number flows, they should also occur in turbulent flows, for example during topological changes. To date, such mechanisms are still largely unexplored. This may be due to the absence of accepted definitions to characterise the lamination within flows and to the high computing cost associated with extensive and detailed characterisation of material elements within complex flows.

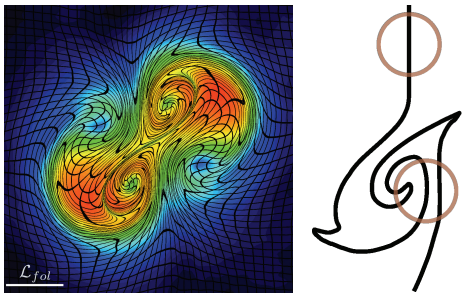

Fig. 1: (left) Superposition of tracked line-tracers initially distributed along a regular grid and the average of the lamination rate intensity along Lagrangian trajectories. (Rossi, 2010). (right) Illustration of the lamination measure which compares the length of the interface included in a centred circle to its diameter. (Rossi and Lardeau, 2011)

A new mechanism to extract folding and lamination rate has recently been proposed (Rossi, 2010) and complemented by a measure of lamination (Rossi and Lardeau, 2011).

The proposed laminating processes rely on the spatial variation of the Lagrangian angular velocity. The Lagrangian angular velocity, $\dot{\theta}$, i.e. the speed of change of direction of the Lagrangian velocity vector, and the direction of rotation, $\mathbf{e}_f$, are defined using a Frenet frame built on the velocity, $\mathbf{u}$, the acceleration perpendicular to the velocity, $\mathbf{a_p}$, and their binormal, $\mathbf{u} \times \mathbf{a_p}$.

$$\dot{\theta} = \sqrt{\frac{\mathbf{a_p} \cdot \mathbf{a_p}}{\mathbf{u} \cdot \mathbf{u}}}, \quad \mathbf{e}_f = \frac{\mathbf{u} \times \mathbf{a_p}}{\|\mathbf{u} \times \mathbf{a_p}\|}$$

The lamination rate $\dot{R}_{fol}$ is then simplified as $\dot{R}_{fol} = \|\boldsymbol{\nabla}\dot{\theta}\|\ell$ where ℓ is a typical length-scale. Fig. 1a illustrates the

good agreement between the lamination estimated using this lamination process (at a given scale indicated as $\mathcal{L}_{fol}$) and the deformation of a grid. Moreover, (Rossi and Lardeau, 2011) show that the lamination rate is larger at small scales and varies as $\dot{R}_{fol} \sim \ell^{-3/4}$.

The measure of lamination, $\mathcal{M}_{lam}$, quantifies the ratio of the total length of an interface within a centred circle to the circle diameter, $\emptyset$, as illustrated in Fig. 1b:

$$\mathcal{M}_{lam} = \frac{1}{\emptyset}\int_{l \in disc} dl$$

(Rossi and Lardeau, 2011) have used this measure to support the coherence of the lamination rate mechanism.

For this study, the authors use the measure of lamination to estimate the typical distance over which the molecular diffusion needs to act to finalise the mixing of a striated structure. Similarly to (Rossi et al., 2011a) we estimate this typical distance as $d = \emptyset/(1 + \mathcal{M}_{lam})$.

In the present paper, first the authors characterise and measure lamination and mixing in a canonical experiment based on a cat's eye flip flow. Second, the same quantification is applied to 2D turbulent flows generated using Direct Numerical Simulations (DNS). Third, we discuss and compare results obtained for canonical and turbulent flows.

EXPERIMENTS, SIMULATIONS AND PROCESSING

Experiments

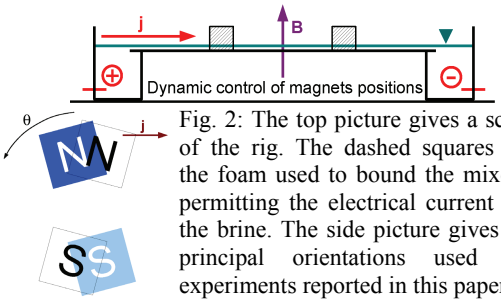

Fig. 2: The top picture gives a schematic of the rig. The dashed squares indicate the foam used to bound the mixer while permitting the electrical current to cross the brine. The side picture gives the two principal orientations used in the experiments reported in this paper.

Experiments are performed in shallow layer brine, 60 g/l NaSO4. The free surface area is about 800mmx600mm. The flow is driven by electromagnetic forces, $\boldsymbol{j} \times \boldsymbol{B}$, generated by the combination of an electrical current, $\boldsymbol{j}$, crossing the brine and square permanent magnets, $\boldsymbol{B}$, of size L_M=40mm. The magnets are placed underneath the brine supporting wall, similarly to (Rossi et al., 2006a, Rossi et al., 2009).

One novelty, since (Rossi et al., 2009) is the dynamic control of the magnets' positions. This is achieved using a three axis robot driven by three servo-motors with independent controllers. The position and orientation of the magnets distribution can then be varied in time. Moreover, the flow domain is reduced to about 200x200mm^2, i.e. $5L_M \times 5L_M$, to study mixing in bounded domain, using plastic (LEGO) walls on two sides and foam on the other sides. The strength of the permanent magnets is B_r=1.2T, the electrical current is I=30mA and the thickness of the brine is about $H = 4.3mm$.

A Particle Image Velocimetry (PIV) method is used to measure the velocity field. The PIV measurements are highly resolved in space with 8.375 pixels per mm. The 16 pixels final correlation windows are about 1.9mm which is more than 20 times smaller than the size of the magnets. The temporal resolution of the experiments is also high. A continuous acquisition at 6Hz allows 285 PIV measurements for each period. As a quasi-steady state is reached after each change of configuration in about 100 pictures, the transient regimes are also well resolved in time. The distance between two points of the PIV grid is of 8 pixels. Taking advantage of a 50% overlap, a standard 3x3 mobile average smoothing is performed on the validated PIV data. The acceleration fields are extracted using the PTVA algorithm (Ferrari and Rossi, 2008) and virtual particle tracking (Rossi et al., 2009). Particle colour methods (Cookson et al., 2009) permitting the measure of entropy and particles concentration, as well as a virtual diffusive dye, i.e. solving scalar transport equation, are also performed using the PIV data.

Numerical simulations of Turbulence

Turbulence is simulated numerically by solving a modified Navier-Stokes equation in a periodic two-dimensional domain of size $2\pi \times 2\pi$. The modification consisting in the replacement of the usual viscous friction by a hyper-diffusivity acting at small-scales, and a hyper-drag at large scales following (Goto and VASSILICOS, 2004). An energy-cascading turbulent velocity field is thus constructed. Advancement of the fields is performed using a vorticity formulation, with a 4th order Runge-Kutta scheme, and pseudo-spectral spatial discretization.

$$\left(\frac{\partial}{\partial t} + \frac{\alpha}{|\mathbf{k}|^2} + \nu|\mathbf{k}|^{16}\right)\hat{\omega}(\mathbf{k}) = -i\mathbf{k}\cdot\mathbf{u}\hat{\omega}(\mathbf{k})$$

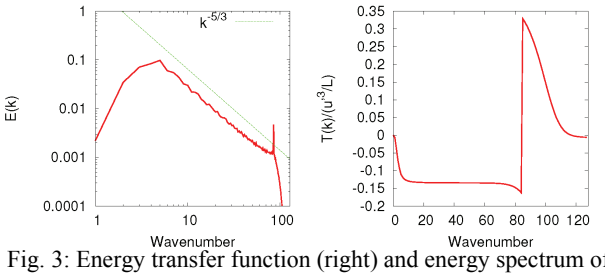

Fig. 3: Energy transfer function (right) and energy spectrum of the turbulent velocity field (left) showing the energy inertial range at scales larger than $k_f = 85$.

Turbulence is sustained by forcing the small scales with the method used in (Goto and VASSILICOS, 2004). With this forcing, the vorticity modulus remains constant in a shell in wavenumber space, with the constraint $|\hat{\omega}(\mathbf{k})| = \omega_0$ for $k_f < |\mathbf{k}| < k_f + 1$. The dissipation operators are chosen specifically to allow a statistically steady, inverse-cascading turbulence: the large scale drag (α term) prevents a pile-up of the energy brought from the forcing scales to large scales, through the energy inertial range, while the hyper-diffusivity ensures that no vorticity inertial range (with a forward cascades from forcing scales to small scales) exists. An inertial range can thus be created between the forcing scale k_f and large scales, as shown by the constancy of the energy transfer function, Fig. 3 (right).

$$T(k) = \sum_{k} \sum_{k'} (\mathbf{u}(\mathbf{k}') \cdot \mathbf{k})(\mathbf{u}(\mathbf{k} - \mathbf{k}') \cdot \mathbf{u}(-k))$$

In this inverse-cascading regime, a self-similar velocity field is sustained, with spectral exponent -5/3, Fig. 3 left.

Numerical simulations of electromagnetically driven flows

Numerical Simulations with electromagnetic body forces are carried out with a finite difference code, using 6th order compact scheme for spatial discretization and 3rd order Runge-Kutta scheme for time derivatives. Poisson equation is solved directly using Fourier decomposition. The forcing model is based on an analytical model (Thibault and Rossi, 2003), considering the 3D distribution of the permanent magnets (Lardeau et al., 2008, Rossi et al., 2009).

Processing

A virtual particle tracking method is used for both lamination and stirring measurements. The tracking is performed using the velocity obtained by PIV measurements and DNS. A Runge Kutta four stage algorithm is used for the advancement in time with a temporal increment ensuring that the maximum displacement is smaller than a quarter of the mesh size.

The line tracking is performed using more than 100 million particles with a maximum distance between two points of the line equals to one tenth of the mesh size.

The spatial average of lamination, its probability distribution and the space filling of the line are computed using a subgrid with a mesh size of a quarter of PIV and DNS meshes. The spatial average of the lamination is computed using the local mean values of the subboxes crossed by the line to remove bias from the local accumulation of lines. The space filling is the number of boxes crossed by the line divided by the total number of boxes.

A particle colour method (Cookson et al., 2009) is used to measure mixing. The mixing is determined by the number of white and black particles in square boxes of about 3x3 pixels. 1 pixel is 8 times smaller than PIV&DNS grids spacing.

The Lorentz body forces are computed according to (Thibault and Rossi, 2003, Lardeau et al., 2008). The values given in Fig. 4 correspond to the mid plane at H/2 from the bottom wall with Br=1.2 T, j=11.6 A/m^2. The distance between the North and South surfaces modelling the magnets is equal to 8cm to consider the magnetic field closure by a thick iron plate.

LAMINATION AND MIXING

Lamination contributes to mixing by its combination with stretching to increase the length of interfaces and its ability to reduce the distance over which diffusion needs to finalise the mixing by increasing striations.

Canonical flow

The canonical flow selected for the present study is a cat's eyes flip sequence at low Reynolds number, i.e. $Re = u_{rms}H/\nu \sim 13$. Fig. 4 gives the distribution of the planar Lorentz body force driving the flow and the corresponding velocity fields measured during the steady forcing and quasi-steady flow configurations. During 22 seconds the flow is forced as on the left column, the orientation of the magnets is then changed (rotation) to reach the second configuration in 1.8s before staying steady for 22s. The pair of magnets is then rotated again in 1.8s to reach the previous orientation. This cycle is then repeated. The forcing period is $T_{flip} = 47.6s$.

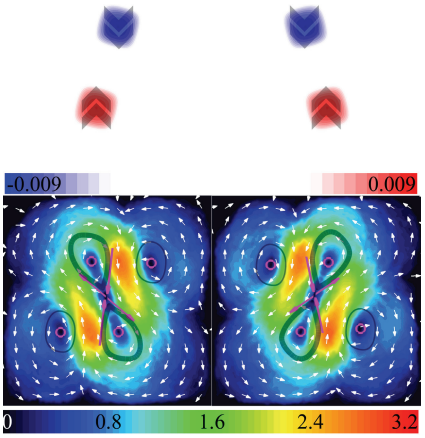

Fig. 4: The first row gives the distribution and direction of the planar Lorentz body force compared to gravity, $\|\mathbf{j}\mathbf{x}\mathbf{B}\|/\rho g$. The second row gives the velocity fields. The colour scale indicates values of $\|\mathbf{u}\|/u_{rms}$ and the plotted arrows the direction of the flow. The purple circles indicate the centre of eddies while the purple arrows denote saddle points and their principal directions.

The velocity fields show flow structures similar to a cat's eyes within a bounded domain. Principal eigen directions near the central hyperbolic stagnation point are indicated by arrows while the centre of recirculation regions, i.e. elliptical stagnation points, are indicated by circles. The typical flow velocity is $u_{rms} = 3.69mm/s$. The typical turnover time associated with the length-scale of the magnets is $L_M/u_{rms} \cong T_{flow} = 11s$. T_{flow} is chosen as the reference time scale for the experiments, $t^* = t/T_{flow}$.The turnover time at the size of the mixer, i.e. $5L_M/u_{rms}$ is about 54s.

Fig. 5 gives the time history of the stirring of a material line and the distribution of a dye generated by particle colour methods. The material line represents the interface between the black and white domains for a non-diffusive dye. This figure shows the stirring processes of the cat's eyes flip mixer. During the steady forcing stages, the flow is stretched in the vicinity of the hyperbolic stagnation point due to higher values of strain in this region. Moreover, it is rolled within elliptical regions. This generates the bending and rolling of the material line, similarly to the illustration given in Fig. 1. When the forcing configuration is changed, the rolling regions and the main direction of stretching are changed. This particular sequence combines the generation of "blinking vortices" with the presence of a hyperbolic region with high strain. In such, it is different and complementary to the "tendril and whorl" and "blinking vortex" sequences previously discussed in literature (Aref, 1984, Khakhar et al., 1986). Moreover, the colour scale indicates the thickness over which the molecular diffusion needs to act to finalise the mixing. This thickness is estimated

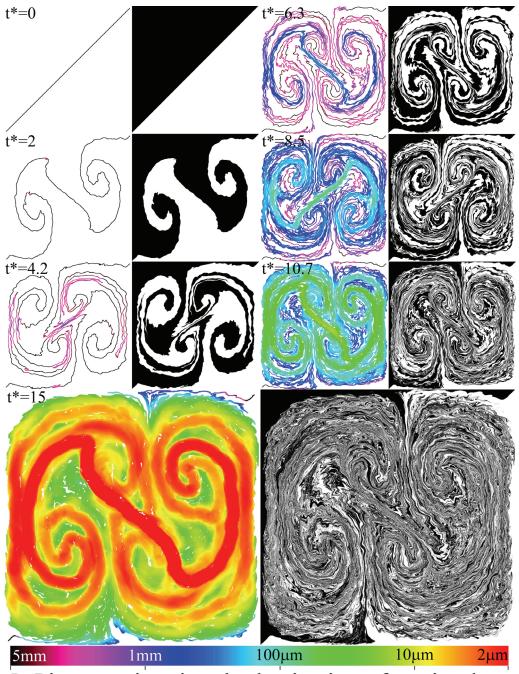

Fig. 5: Picture pairs give the lamination of a stirred material line (left) and the stirring of a virtual dye (right) generated by particle colour methods. The logarithmic colour scale indicates the typical striations thickness. $t^* = t/T_{flow}$.

using the measurement of lamination along the material line, as discussed in the introduction section. First, this thickness is strongly reduced. After only 15 turnover times, it has been globally divided by about one hundred, reducing the diffusion time by ten thousands. Also, the local process leading to a decrease of this thickness (respectively increase of lamination) near the hyperbolic stagnation point can be pointed out. For example, at time $t^* = 8.5$ there is a local accumulation of lines within this region. This combination of higher lamination with continuous stretching generates the orange-red pattern at time $t^* = 15$ where the diffusion thickness has been reduced by one thousand, reducing the diffusion time by one million.

To quantify the action of this mixer, the relative length of the material line, L/L_0, where L_0 is the initial length of the line, and the spatial average of the lamination, preventing bias from local accumulation of lines, are measured. Those values are plotted in semi-log versus time in Fig. 6. Both stretching and lamination grow exponentially with similar exponents. Computations for different line orientations show that the stretching grows as $\sim e^{3^{\pm 1.1\%} t/T_{flip}}$ and the lamination as $\sim e^{2.70^{\pm 0.8\%} t/T_{flip}}$. This is characteristic of a baker process where lamination and stretching complement each other to produce an exponential growth of interfaces.

To complement these stirring statistics, the mixing coefficient of the dye is plotted versus time in Fig. 7. The mixing coefficient is the rescaled variance, $(\sigma_{max}^2 - \sigma^2)/(\sigma_{max}^2 - \sigma_{meas}^2)$, where σ^2 is the variance of the dye distribution, σ_{max}^2=0.25 and σ_{meas}^2=0.013 to consider the discrete sampling of the particles. As highlighted by the semi-log insert, the rapid initial growth of the mixing coefficient corresponds to an exponential growth. After height turnover times, $t^* > 8$, the stirring process starts to pursue mixing in regions where the dye is already mixed while other regions are still to be mixed. This is illustrated by the grey colour on Fig. 5 for $t^* = 15$. Moreover, the measurement of particle concentration is performed within boxes of about 363µm side, i.e. $0.009L_M$. For $t^* > 8$, Fig. 5 shows that the typical striations' thickness start to be smaller than 363µm in growing parts of domain. Consequently, such regions appear mixed.

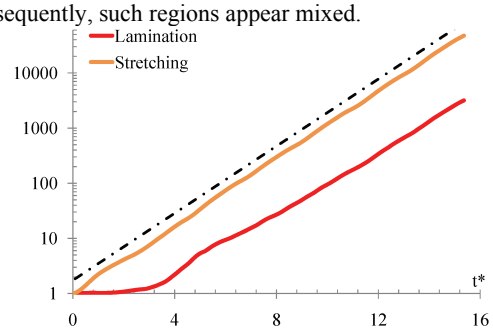

Fig. 6: Spatial average lamination and stretching L/L_0 of a material line during cat's eyes flip flow. The lamination measurement is done with a circle of 1cm diameter.

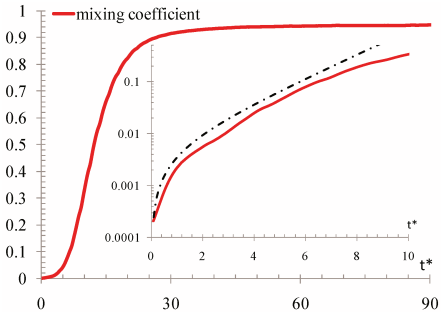

Fig. 7: mixing coefficient, $(\sigma_{max}^2 - \sigma^2)/(\sigma_{max}^2 - \sigma_{meas}^2)$, versus $t^*$for the cat's eyes flip flow. The dot-dash, line on the semi-log insert, corresponds to $0.005\left(e^{2.2t^*} - 1\right)$.

Turbulent flow

The same characterisation is applied to a turbulent flow generated by DNS. The present simulations have a forcing wave number $k_f = 85$, with $\omega_0 = 0.5$, hyper-drag coefficient α=0.25 and hyper-diffusivity ν=3 10^{-31}. The resulting velocity field has u_{rms}=1.85, with integral scale $\mathcal{L}$=0.86. About 185 velocity fields are exported per large-scale turnover time, $T_{turb} = \mathcal{L}/u_{rms} \cong 0.462$ which is chosen as the reference time-scale, $t^+ = t/T_{turb}$

Fig. 8 gives the time history of a material line, coloured according to the local distance over which the diffusion needs to act to finalise mixing, and a dye generated with particle colour methods. The line is stretched and laminated by the turbulent flow. Moreover, within four large scale turnover times, $t^+ = 4$, the typical diffusive distance is locally divided by one thousand, locally reducing the diffusion time by one million. Also, the stretching and dispersion of some subsets of black dye can be observed. Some black patches/bands are becoming grey and then disappearing when the concentration of black particles is below a few percents.

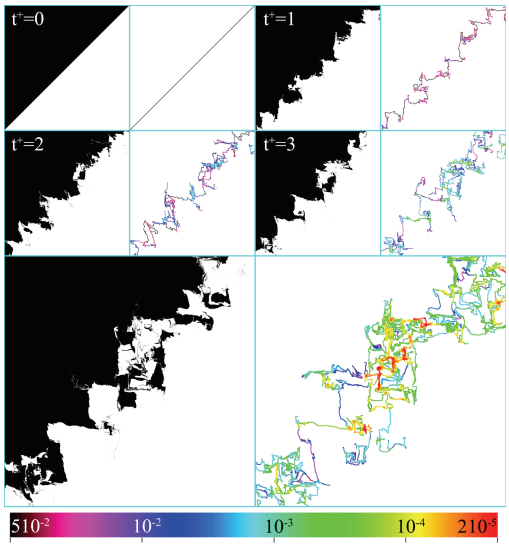

Fig. 8: Picture pairs give the lamination of a stirred material line (left) and the stirring of a virtual dye (right) generated by particle colour methods. The logarithmic colour scale indicates the typical striations thickness, $d^+ = d/\mathcal{L}$.

Fig. 9 gives, in a semi-log plot, the stretching and lamination statistics of the material line illustrated in Fig. 8. Both stretching and lamination grow exponentially in time with different exponents. Computations for different lines (varying orientations) show that the stretching grows as $\sim e^{2.39^{\pm 8.4\%} t^+}$ and the lamination as $\sim e^{1.81^{\pm 6.1\%} t^+}$.

The exponential growth of a material line within turbulent flows was predicted by (Batchelor, 1952) and previously observed in numerical simulations, e.g. (Girimaji and S.B., 1990, Goto and Kida, 2007).

The measure of lamination within turbulent flows according to (Rossi and Lardeau, 2011) is to the knowledge of the authors a new result which shows the presence of lamination within turbulent flows. Moreover, the exponential growth of the lamination spatial average (removing bias from local accumulation of lines) at first suggests the presence of a baker process while such a process is generally considered as a property of low Reynolds number flows.

Fig. 10 gives the evolution of the mixing coefficient, in log-log. Whilst the exponential growth of lamination supports the presence of a baker process, the growth of the mixing coefficient is algebraic. This is clearly different from a baker-like mixing process, as expected in turbulent flows. Also, this power law growth has an exponent close to 1.25, as previously observed in literature, e.g. (Beta et al., 2003).

Discussion

The authors now discuss and attempt to fairly compare the results obtained for low Reynolds number and turbulent flows. For this comparison, the large-scale turnover time and the period of forcing are chosen as time-scale reference. Moreover, the authors consider that the turbulent stirring mainly occurs within a diagonal band of thickness $\mathcal{L}\sqrt{2}$ made of overlapping $\mathcal{L} \times \mathcal{L}$ boxes.

Both canonical and turbulent flows present exponential growth for the stretching and lamination of a material line, with an exponent higher for the stretching than for the lamination. The difference between the exponents is larger in the turbulent case. Indeed, the presence of pure strain within flows can generate an exponential growth of material line without the need of baker-like processes. The combination of pure strain and lamination leads to an exponential growth higher for the line stretching than for the lamination. This can be written as $L/L_0 \sim e^{(\lambda_{strain}+\beta_{baker})t}$, where $e^{\beta_{baker} t}$ is the exponential growth of the lamination.

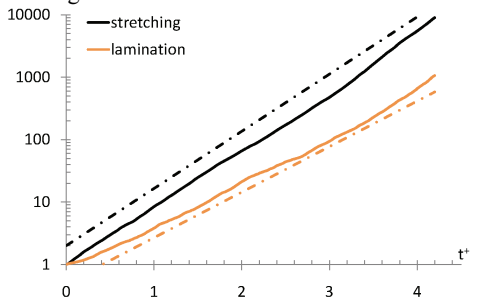

Fig. 9: stretching L/L_0 and average lamination of a material line within the turbulent flow. The lamination measurements are done with a circle of diameter $\phi = 0.1\mathcal{L}$. $t^+ = t/T_{turb}$

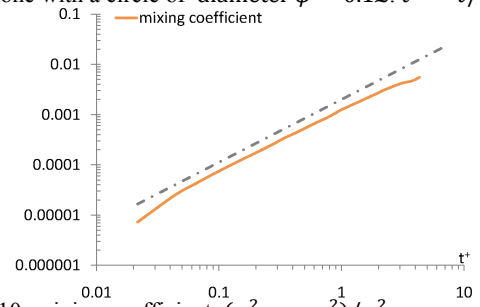

Fig. 10: mixing coefficient, $(\sigma_{max}^2 - \sigma^2)/\sigma_{max}^2$, versus t^+, for the turbulent flow. The dash-dot line indicates a power law with an exponent of 1.2.

Despite these exponential growths, the mixing properties of the canonical flow and the turbulent flow differ.

Fig. 11 gives the space filling of these two flows. The maximum scale of the turbulent statistic is set to 0.2 and not 1 to ensure fair comparison. As it could be guessed from Fig. 5 and Fig. 8, the space filling statistic confirms that the cat's eyes flip has better filling properties than the turbulent flow.

Fig. 12 gives the probability distribution (pdf) of the lamination for the cat's eyes and turbulent flows at $t^+ = 4.2$ and $t/T_{flip} = 3.6$. Both pdf could be simplified as a regular increase of the probability, i.e. first power law with positive exponent, followed by a drop towards large values of the lamination, i.e. second power law with a negative exponent. The main difference is that the most likely lamination is one order of magnitude lower than the mean lamination for the turbulent flow while it is of the same order of magnitude for the cat's eyes flow. These distributions show that lamination mainly occurs locally with high intensity in the case of a turbulent flow while it is globally built in the case of the cat's eyes flow.

These results show that in the case of a turbulent flow the lamination enhances the mixing locally while this locality saturates the baker like process with a reduced the space filling. According to the increase of lamination rate and strain (local accumulation of lines) with the reduction of scales, it is likely that this process is mainly driven by the small scales in ordinary turbulent flows.

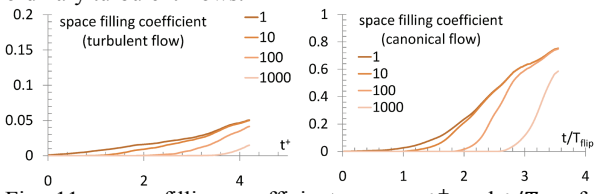

Fig. 11: space filling coefficients versus t^+ and t/T_{flip} for different values of laminations (1, 10, 100 and 1000). The turbulent and cat's eyes flip flows are on the left and right

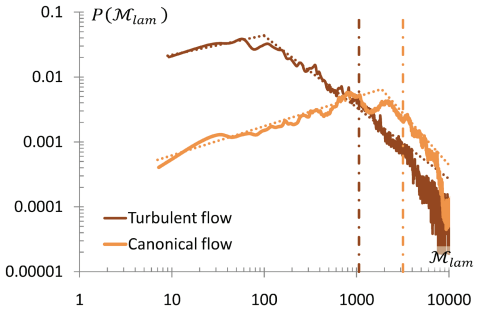

Fig. 12: Probability distribution of lamination for the turbulent and cat's eyes flip flows at $t^+ = 4.2$ and $t/T_{flip} = 3.6$. Dot-dash vertical lines indicate the mean values.

CONCLUSION:

The authors have shown that the cat's eyes flip and the turbulent flow both present stretching and lamination growing exponentially in time. Nevertheless, their mixing properties are different, the canonical flow being exponential (before saturation) and the turbulent flow algebraic. Moreover, the distribution of lamination strongly differs between these two mixers. This may explain the early saturation of the turbulent mixer when compared to the cat's eyes flip mixer. Finally, the cat's eyes flip is simply generated by changes in the distribution of two counter jets while the cat's eyes structure is one of the key structures observed in 2D turbulent flows. It is tempting to consider that turbulent flows may not be ideal (or best) mixers and that lamination processes should be explored further to design new turbulent mixers.

The authors acknowledge the EPSRC grant EP/D072034/1.

References

AREF, H. 1984. Stirring by chaotic advection. *Journal of Fluid Mechanics Digital Archive,* 143, 1-21.

BATCHELOR, G. K. 1952. The effect of homogeneous turbulence on matrial lines and surfaces. *Proc. R. Soc. Lond. A,* 213, 349-366.

BETA, C., SCHNEIDER, K., FARGE, M. & BOCKHORN, H. 2003. Numerical study of mixing of passive and reactive scalars in two-dimensional turbulent flows using orthogonal wavelet filtering. *Chemical Engineering Science,* 58, 1463-1477.

COOKSON, A. N., DOORLY, D. J. & SHERWIN, S. J. 2009. Mixing Through Stirring of Steady Flow in Small Amplitude Helical Tubes. *Annals of Biomedical Engineering,* 37, 710-721.

FERRARI, S. & ROSSI, L. 2008. Particle tracking velocimetry and accelerometry (PTVA) measurements applied to quasi-two-dimensional multi-scale flows. *Exp. Fluids,* 44, 873-886.

GIRIMAJI, S. S. & S.B., P. 1990. Material-element deformation in isotropic turbulence. *J . Fluid Mech.,* 220, 427-458.

GOTO, S. & KIDA, S. 2007. Reynolds-number dependence of line and surface stretching in turbulence: folding effects. *J. Fluid Mech.,* 586.

GOTO, S. & VASSILICOS, J. C. 2004. Particle pair diffusion and persistent streamline topology in two-dimensional turbulence. *New Journal of Physics,* 6, 1-35.

KHAKHAR, D. V., RISING, H. & OTTINO, J. M. 1986. Analysis of chaotic mixing in two model systems. *Journal of Fluid Mechanics Digital Archive,* 172, 419-451.

LARDEAU, S., FERRARI, S. & ROSSI, L. 2008. Three-dimensional direct numerical simulation of electromagnetically driven multiscale shallow layer flows: Numerical modeling and physical properties. *Phys. Fluids,* 20, 127101.

REYNOLDS, O. 1893. Study of Fluid Motion by means of Coloured Bands. *Proceedings of the Royal Institution of Great Britain,* XIV, 129-138.

ROSSI, L. 2010. A mechanism to explore lamination rates. *Phys. Rev. E.,* 81, 027301.

ROSSI, L., BOCQUET, S., FERRARI, S., GARCIA DE LA CRUZ, J. M. & LARDEAU, S. 2009. Control of flow geometry using electromagnetic body forcing. *International Journal of Heat and Fluid Flow,* 30, 505-513.

ROSSI, L., DOORLY, D. & KUSTRIN, D. 2011a. Lamination and mixing in laminar flows driven by Lorentz body forces. *Nature (submitted)*.

ROSSI, L., KUSTRIN, D. & DOORLY, D. 2011b. Lamination and mixing in canonical flows driven by electromagnetic body forces. *Phys. Rev. Lett. (submitted)*.

ROSSI, L. & LARDEAU, S. 2011. Lamination and folding in electromagnetically driven flows of specified geometries. *Journal of Turbulence,* 12, N6.

ROSSI, L., VASSILICOS, J. C. & HARDALUPAS, Y. 2006a. Electromagnetically controlled multi-scale flows. *J. Fluid Mech.,* 558, 207 - 242.

ROSSI, L., VASSILICOS, J. C. & HARDALUPAS, Y. 2006b. Multiscale Laminar Flows with Turbulentlike Properties. *Phys. Rev. Lett.,* 97, 144501.

THIBAULT, J.-P. & ROSSI, L. 2003. Electromagnetic flow control: characteristic numbers and flow regimes of a wall-normal actuator. *J. Phys. D: Applied Physics*, 2559-2568.

WIGGINS, S. & OTTINO, J. M. 2004. Foundations of chaotic mixing. *Philosophical Transactions of the Royal Society of London. Series A: Mathematical, Physical and Engineering Sciences,* 362, 937-970.